Supporting Information for:

Triphase Interface Synthesis of Plasmonic Gold Bellflowers as Near-infrared Light Mediated Acoustic/Thermal Theranostics

Peng Huang,[1§] Pengfei Rong,[1,2,4§] Jing Lin,[1] Wanwan Li,[1] Xuefeng Yan,[1] Molly Gu Zhang,[1] Liming Nie,[1,3] Gang Niu,[1] Jie Lu,[1] Wei Wang,[4] Xiaoyuan Chen[1]*

[1]Laboratory of Molecular Imaging and Nanomedicine (LOMIN), National Institute of Biomedical Imaging and Bioengineering (NIBIB), National Institutes of Health, Bethesda, Maryland 20892, United States

[2]State Key Laboratory for Powder Metallurgy, Central South University, Changsha, Hunan 410083, China

[3]Center for Molecular Imaging and Translational Medicine, State Key Laboratory of Molecular Vaccinology and Molecular Diagnostics, School of Public Health, Xiamen University, Xiamen 361005, China

[4]Department of Radiology, The Third Xiangya Hospital, Central South University, Changsha, Hunan 410013, PR China

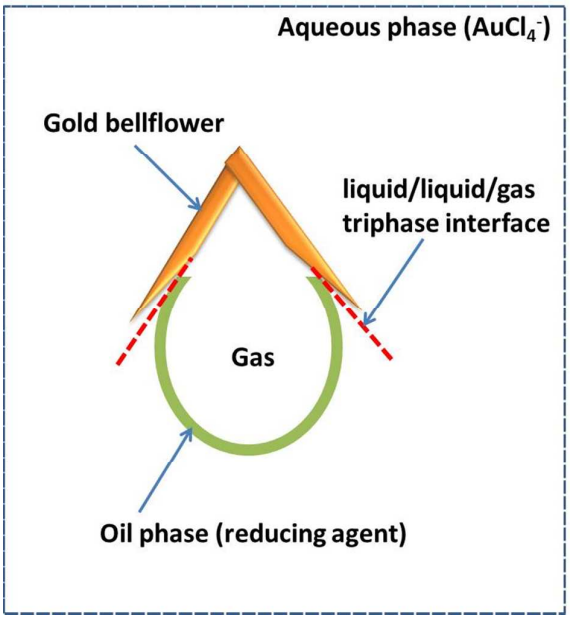

Scheme S1 The growth mechanism of GBFs. Outward flange bubble as an exmaple. reacted molecular precursors were spatially separated in the hexane/toluene (reducing agent) and aqueous phases ($AuCl_4^-$). Upon ultrasound irradiation, due to the cavitation and nebulization between ultrasound and solvent media, the redox reaction was mostly occurred along the liquid/liquid/gas triphase interface with extremely high temperature and pressure.

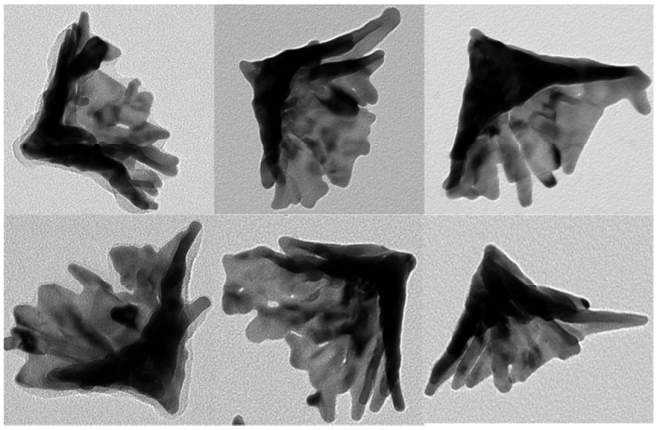

Figure S1. Side View TEM images of individual GBFs.

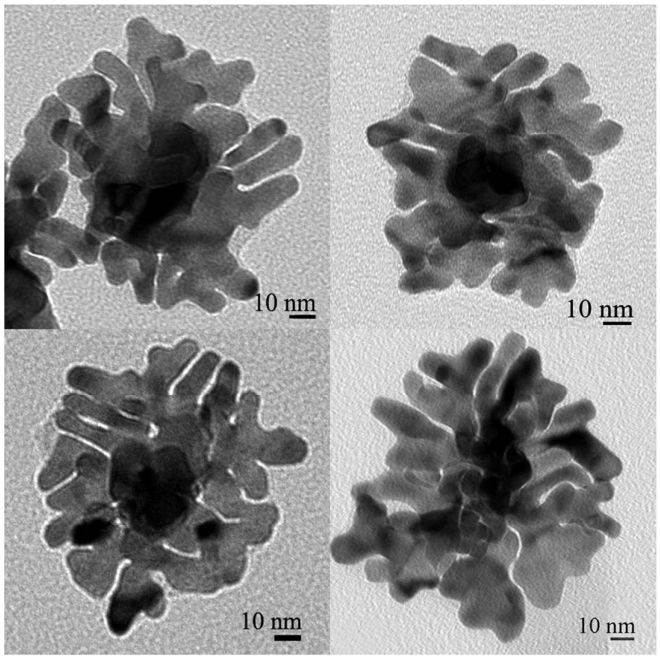

Figure S2. Top View TEM images of individual GBFs.

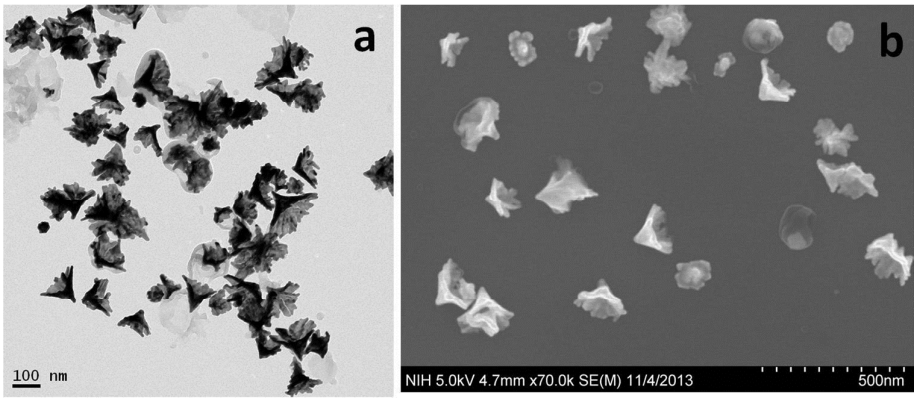

Figure S3. Low magnification TEM (a) and SEM (B) images of GBFs.

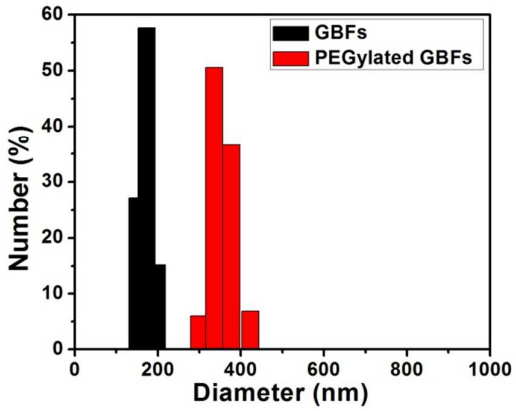

Figure S4. Size distributions of GBFs and PEGylated GBFs measured by dynamic light scattering (DLS).

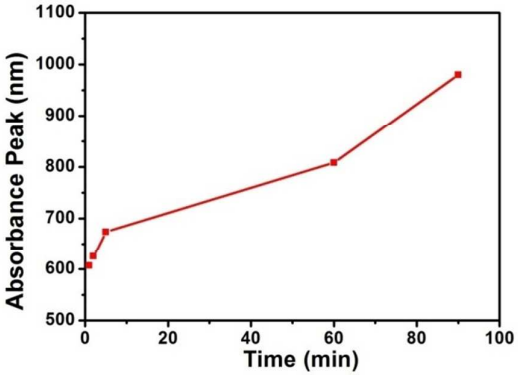

Figure S5. Time-dependent LSPR peak changes of GBFs.

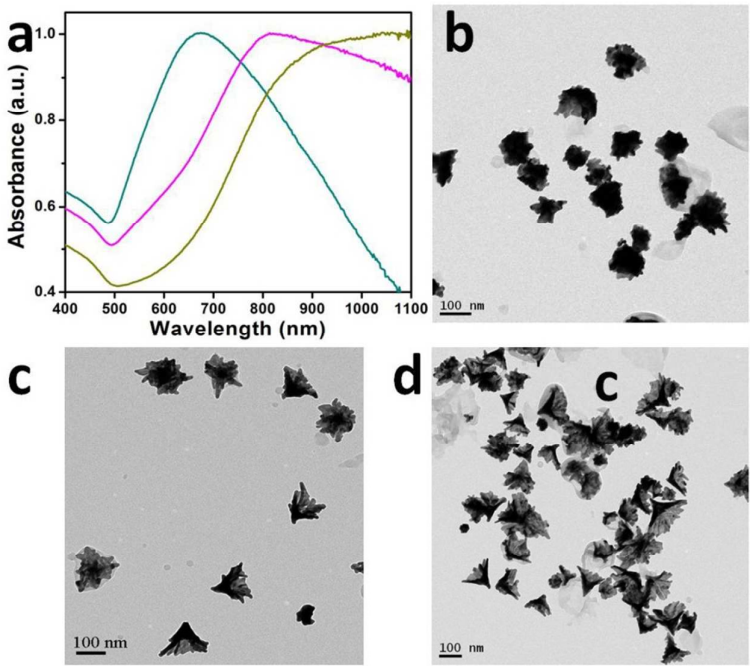

Figure S6. (a) UV-vis-NIR absorbance spectra of GBFs at 5, 60, and 90 min, and (b-d) the corresponding TEM images.

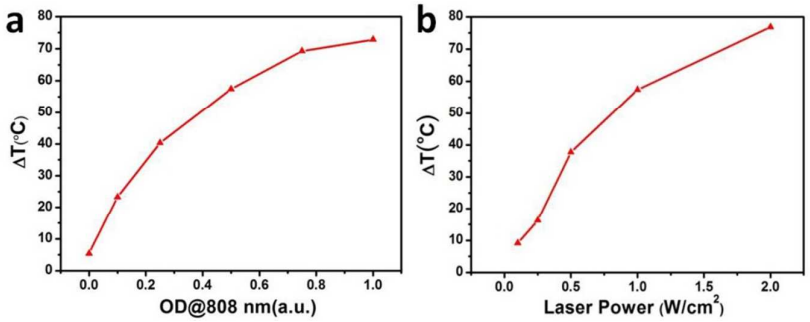

Figure S7. (a) Plot of temperature change (ΔT) of aqueous solution of GBFs with the same laser power density of 1 W/cm^2 and different optical densities (ODs) at 808 nm; (b) Plot of temperature change (ΔT) of aqueous solution of GBFs with OD@808 nm equals to 0.5 irradiated by different laser power densities.

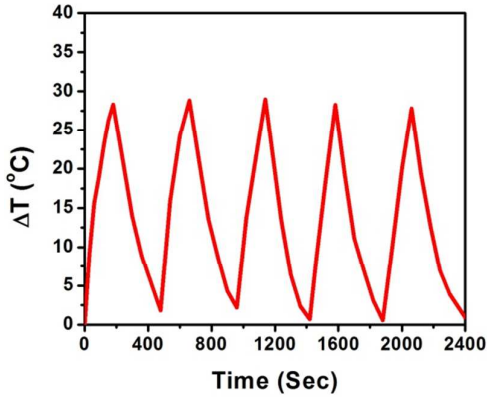

Figure S8. Plot of temperature change (ΔT) of GBFs solution (OD@808 nm = 0.5) irradiated by an 808 nm laser (0.5 W/cm^2) for five on/off cycles (on: 3 min, off: 5 min).

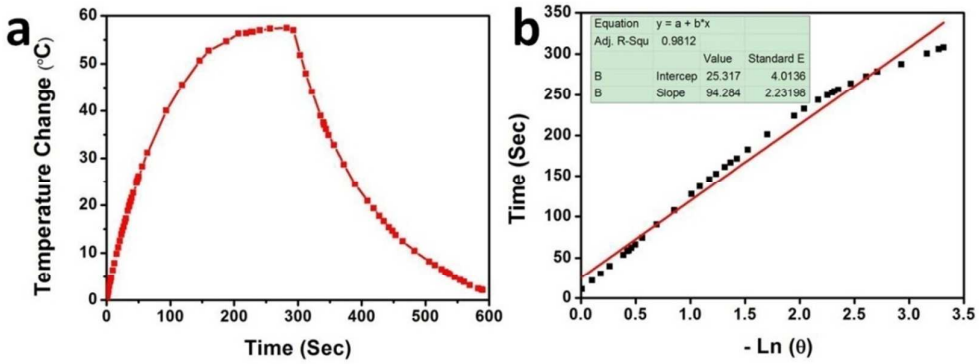

Figure S9. (a) Photothermal effect of the irradiation of the aqueous dispersion of BGVs (OD@808 nm = 0.5) with the NIR laser (808 nm, 1 W/cm^2), in which the irradiation lasted for 5 min, and then the laser was turned off. (b) Time constant for heat transfer from the system is determined to be τs = 94.28 s by applying the linear time data from the cooling period (after 300 s) versus negative natural logarithm of driving force temperature, which is obtained from the cooling stage of panel a.

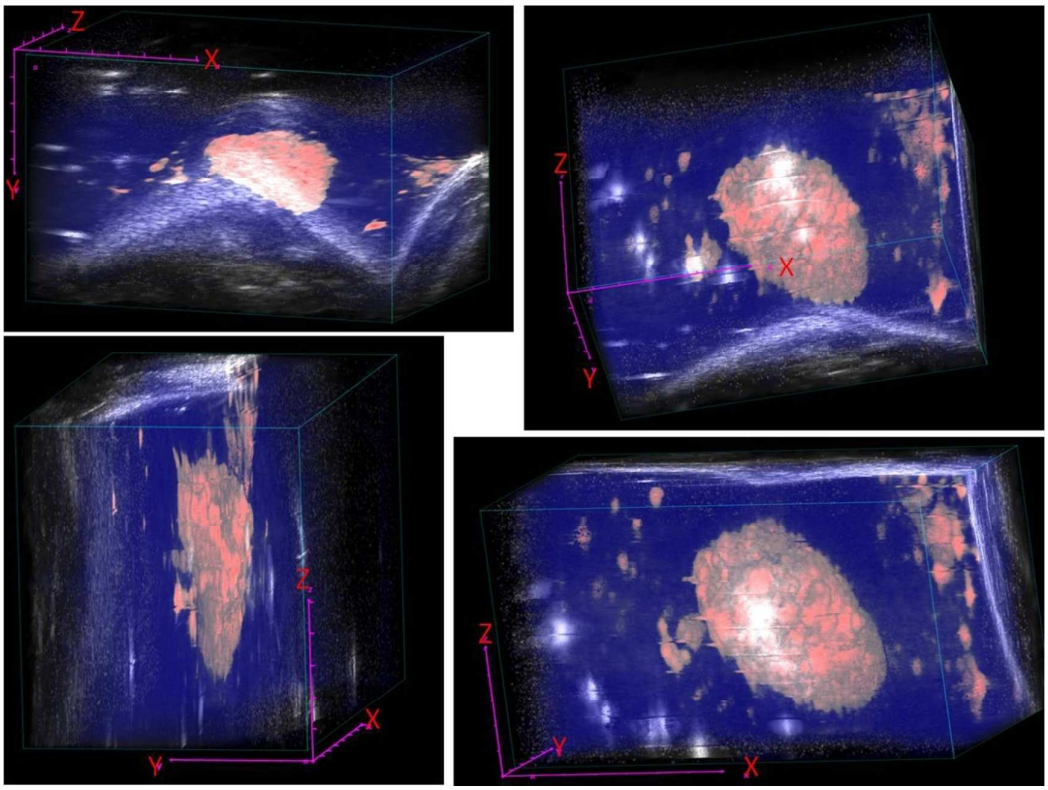

Figure S10. *In vivo* photoacoustic (PA) images of tumor tissue after intratumoral injection.

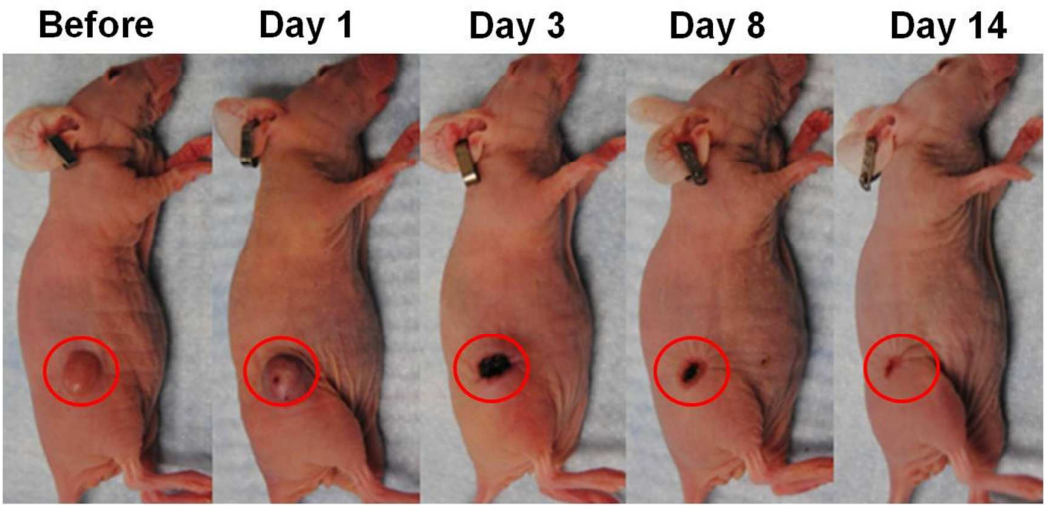

Figure S11. Typical time dependent variation photographs of 4T1 tumor-bearing mice with GBFs (400 μg/mL, 50 μL) injection after exposed to the 808 nm laser at power density of 0.5 W/cm^2 for 5 min.

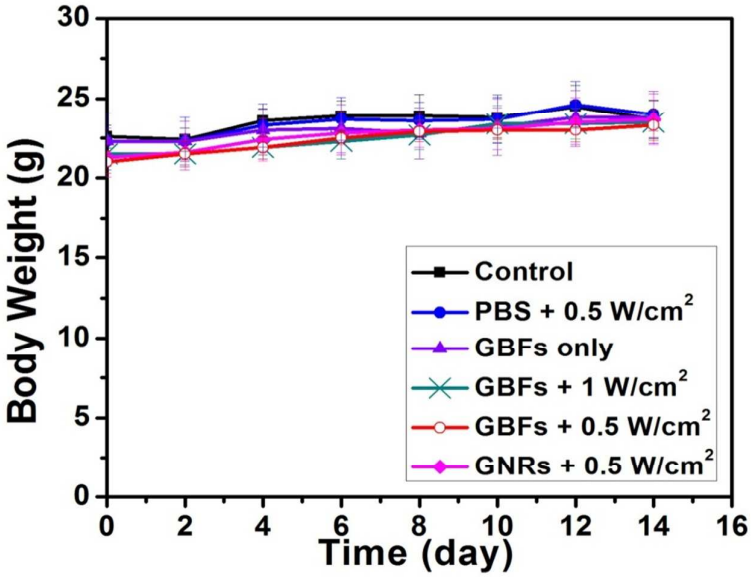

Figure S12. Mice body weight changes of tumor-bearing mice after various treatments indicated. The body weight of mice did not show significant change over 2 weeks, indicating the excellent biocompatibility of GBFs in vivo.

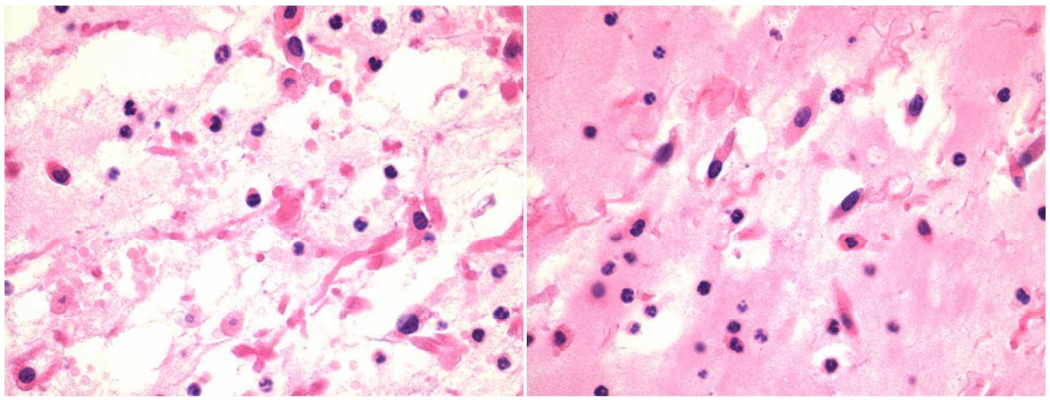

Figure S13. H&E stained images (40 x) of tumor section collected from GBFs/laser group of mice at day1.

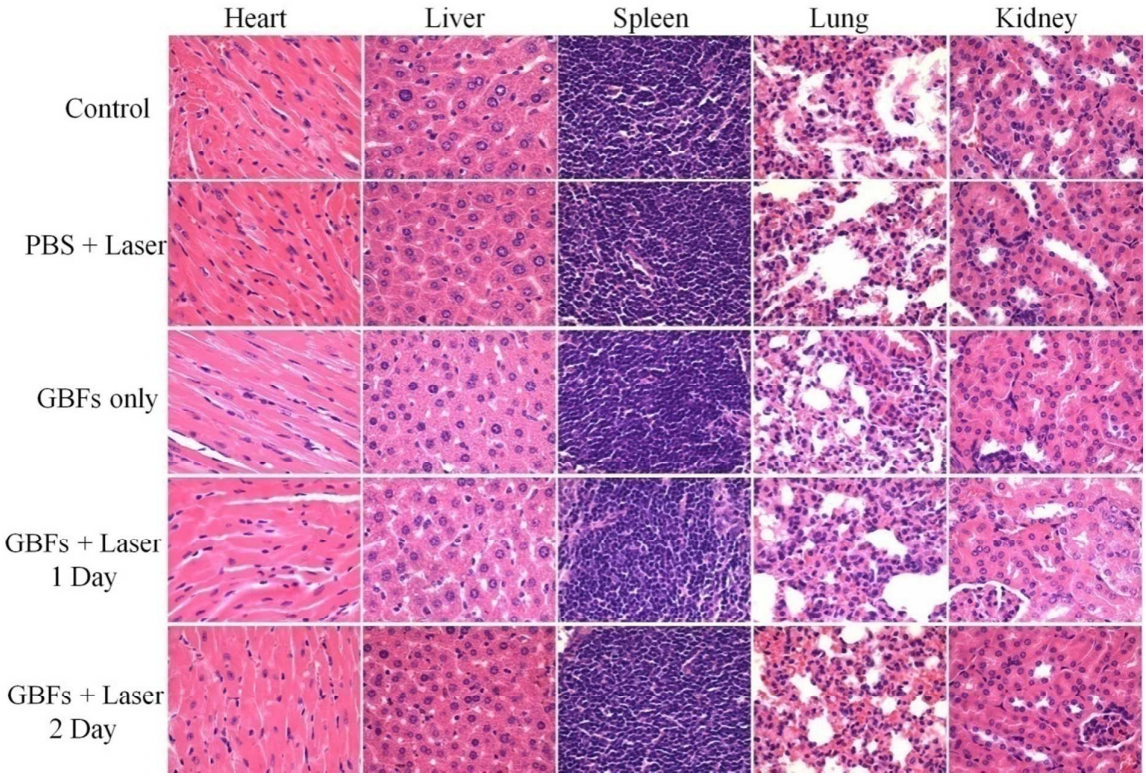

Figure S14. H&E stained images of major organs collected from different groups of mice.

Table S1 Photothermal conversion efficiency of GBFs comparing with various nanomaterials.

Photothermal conversion agents	Photothermal conversion efficiency (η)	Wavelength (nm)	References
Gold Nanoshells	13%	800	[51]
Gold Vesicles	18%	808	[5, 71]
Gold Nanorods	22%	808	[5]
Gold Hexapods	29.6%	808	[39]
Biodegradable Gold Vesicles	37%	808	[5]
Gold Nanocages	63%	808	[39]
Gold Bellflowers	**74%**	**808**	This study
$Cu_{2-x}Se$ Nanocrystals	22%	800	[51]
Cu_9S_5 Nanocrystals	25.7%	980	[48]
Fe_3O_4@$Cu_{2-x}S$ Nanocrystals	16%	980	[49]
Dopamine-melanin Nanospheres	40%	808	[50]